universe MDPI

Communication

Beam Energy Dependence of the Linear and Mode-Coupled Flow Harmonics Using the a Multi-Phase Transport Model

Niseem Magdy

Department of Chemistry, State University of New York, New York, NY 11794, USA; niseemm@gmail.com

Abstract: In the framework of the A Multi-Phase Transport (AMPT) model, the multi-particle azimuthal cumulant method is used to calculate the linear and mode-coupled contributions to the quadrangular flow harmonic (v_4) and the mode-coupled response coefficient as functions of centrality in Au+Au collisions at $\sqrt{s_{NN}}$ = 200, 39, 27 and 19.6 GeV. This study indicates that the linear and mode-coupled contributions to v_4 are sensitive to beam energy change. Nevertheless, the correlations between different-order flow symmetry planes and the mode-coupled response coefficients show weak beam energy dependence. In addition, the presented results suggest that the experimental measurements that span a broad range of beam energies can be an additional constraint for the theoretical model calculations.

Keywords: collectivity; correlation; shear viscosity

check for updates

Citation: Magdy, N. Beam Energy Dependence of the Linear and Mode-Coupled Flow Harmonics Using the a Multi-Phase Transport Mode. *Universe* **2023**, *9*, 107. https://doi.org/10.3390/universe9020107

Academic Editors: Jun Xu and Yingxun Zhang

Received: 12 January 2023
Revised: 8 February 2023
Accepted: 16 February 2023
Published: 18 February 2023

1. Introduction

Experimental investigations of heavy-ion collisions demonstrate the formation of Quantum Chromodynamic (QCD) matter called Quark–Gluon Plasma (QGP) at the Relativistic Heavy Ion Collider (RHIC) and Large Hadron Collider (LHC) [1–3]. One of the primary purposes of previous and present experimental studies of heavy-ion collisions is to understand the QGP transport properties, such as shear viscosity divided by entropy density, η/s [4–10].

In recent years, experimental measurements of anisotropic flow resumed being a beneficial route to the extraction of η/s [5,11–23]. In addition, anisotropic flow gives the viscous hydrodynamic response to the initial-state energy density anisotropy described by complex eccentricity vectors $\mathcal{E}_n$ [24–28].

$$\begin{aligned} \mathcal{E}_n &\equiv \varepsilon_n e^{in\Phi_n} \qquad (1)\\ &\equiv -\frac{\int dx\, dy\, r^n\, e^{in\varphi}\, E(r,\varphi)}{\int dx\, dy\, r^n\, E(r,\varphi)},\ (n\ >\ 1), \\ x &= r\ \cos\varphi, \qquad (2)\\ y &= r\ \sin\varphi, \qquad (3) \end{aligned}$$

where ε_n and Φ_n are the magnitude and the angle of the nth-order eccentricity vector, φ is the spatial azimuthal angle and $E(r,\varphi)$ is the initial anisotropic energy density profile [27,29,30].

The anisotropic flow can be given by the Fourier expansion of the azimuthal anisotropy of particles emitted relative to the collision symmetry planes [31].

$$E\frac{d^3N}{d^3p} = \frac{1}{2\pi}\frac{d^2N}{p_T dp_T dy}\left(1 + \sum_{i=1}^{\infty} 2v_n \cos(n(\phi - \psi_m))\right), \qquad (4)$$

where v_n stands for the n^{th} flow coefficient, y is the rapidity, ϕ represents the particle azimuthal angle, p_T gives the transverse momentum and ψ_m is the m^{th}-order symmetry plane. Flow harmonics v_n (n = 1, 2 and 3) are called directed, elliptic and triangular flow, respectively.

Prior and current studies of v_2 and v_3 suggest that to a reasonable degree, they are linearly related to the medium response [28,32–41].

$$v_n = \kappa_n \varepsilon_n, \tag{5}$$

where κ_n (for n = 2 and 3) encodes the importance of QGP η/s [42,43]. Higher-order flow harmonic v_4 [19,34,38,42,44–47] exhibits a linear response to same-order eccentricity as well as a mode-coupled response to lower-order eccentricity ε_2 [21,29,30,48].

$$\begin{aligned} V_4 &= v_4 e^{i4\psi_4} = \kappa_4 \varepsilon_4 e^{4i\Phi_4} + \kappa_4' \varepsilon_2^2 e^{4i\Phi_2} \\ &= V_4^{\rm Linear} + \chi_{4,22} V_4^{\rm MC}, \end{aligned} \tag{6}$$

where κ_4' represents the mixed effect of the medium properties and the coupling between lower- and higher-order eccentricity harmonics. $V_4^{\rm Linear}$, $V_4^{\rm MC}$ and $\chi_{4,22}$ are the linear and the mode-coupled contributions to V_4 and the mode-coupled response coefficients, respectively.

The mode-coupled response to V_4 represents additional constraints for initial-stage dynamics and η/s extraction [29,32,33,37,49–54]. Therefore, ongoing work suggests that leveraging comprehensive measurements of $v_4^{\rm Linear}$ and $v_4^{\rm MC}$ could provide additional constraints to differentiate between various initial-state models [9,10,32,55]. In addition, these measurements could pin down the η/s dependence on temperature (T) and baryon chemical potential (μ_B).

The paper is organized as follows: Section 2 describes the AMPT model and the analysis technique employed in this work. Section 3 conveys the results of this work. The summary is presented in Section 4.

2. Method

AMPT [56] model (version ampt-v2.26t9b)-simulated events were used in the present investigation of Au+Au collisions at $\sqrt{s_{NN}}$ = 200, 39, 27 and 19.6 GeV. The used AMPT model has both string-melting mechanism and hadronic cascade turned on. The AMPT model has been widely employed to investigate relativistic heavy-ion collision physics [56–65]. In the AMPT model with string melting on, the HIJING model is used for hadron creation. These hadrons are then transformed into their valence quarks and anti-quarks. In addition, their time and space evolution is evaluated with the ZPC parton cascade model [66].

The AMPT has four essential components: (i) the HIJING model [67,68] in the initial parton production stage, (ii) the parton scattering stage and (iii) hadronization through coalescence, followed by (iv) a hadronic interaction stage [69]. In the stage of parton scattering, the parton scattering cross-section is given as

$$\sigma_{pp} = \frac{9\pi\alpha_s^2}{2\mu^2}, \tag{7}$$

where μ = 4.6 gives the partonic matter screening mass and α_s = 0.47 represents the QCD coupling constant. Parameters μ and α_s generally give the expansion dynamics of A–A collision systems [66,70–72]. In the current work, σ_{pp} was fixed to 1.5 mb.

In the current work, the centrality intervals were obtained by cutting on the charged particle multiplicity in midrapidity. Then, the AMPT-simulated events were analyzed using the multi-particle cumulant method [49,73–75] using particles with pseudorapidities $|\eta| < 1$ and with transverse momentum $0.2 < p_T < 2.0$ GeV/c.

The multi-particle cumulant technique was here used for correlation analysis. The framework of the multi-particle cumulant using one and many sub-events is described in Refs. [49,73–75]. Here, I used two-, three- and four-particle correlations in this work by applying the two-sub-event cumulant technique [74]. The two sub-events A and B with

$|\Delta\eta| > 0.7$ (i.e., $\eta_A > 0.35$ and $\eta_B < -0.35$) were used. Using the two-sub-event method helps reduce non-flow correlations [76]. Two-, three- and four-particle correlations are given using the two-sub-event cumulant method [74] as

$$v_n^{\text{Inclusive}} = v_n = \langle\langle \cos(n(\varphi_1^A - \varphi_2^B))\rangle\rangle^{1/2}, \tag{8}$$

$$C_{n+m,nm} = \langle\langle \cos((n+m)\varphi_1^A - n\varphi_2^B - m\varphi_3^B)\rangle\rangle, \tag{9}$$

$$\langle v_n^2 v_m^2 \rangle = \langle\langle \cos(n\varphi_1^A + m\varphi_2^A - n\varphi_3^B - m\varphi_4^B)\rangle\rangle, \tag{10}$$

where $\langle\langle\,\rangle\rangle$ represents the average over all particles and all events, and φ_i is the i^{th} particle azimuthal angle.

Using Equations (8)–(10), the mode-coupled response to v_{n+m} is [30,77]

$$\begin{aligned} v_{n+m}^{\text{MC}} &= \frac{C_{n+m,nm}}{\sqrt{\langle v_n^2 v_m^2 \rangle}}, \\ &\sim \langle v_{n+m} \cos((n+m)\Psi_{n+m} - n\Psi_n - m\Psi_m)\rangle. \end{aligned} \tag{11}$$

Moreover, the linear response to v_{n+m} is

$$v_{n+m}^{\text{Linear}} = \sqrt{(v_{n+m}^{\text{Inclusive}})^2 - (v_{n+m}^{\text{MC}})^2}. \tag{12}$$

The ratio of the mode-coupled response to inclusive v_{n+m} gives the correlations between different-order flow symmetry planes.

$$\begin{aligned} \rho_{n+m,nm} &= \frac{v_{n+m}^{\text{MC}}}{v_{n+m}^{\text{Inclusive}}}, \\ &\sim \langle \cos((n+m)\Psi_{n+m} - n\Psi_n - m\Psi_m)\rangle. \end{aligned} \tag{13}$$

The mode-coupled response coefficient gives the coupling to the higher-order anisotropic flow harmonics and is given as

$$\chi_{n+m,nm} = \frac{v_{n+m}^{\text{MC}}}{\sqrt{\langle v_n^2\, v_m^2 \rangle}}. \tag{14}$$

3. Results and Discussion

Extracting the linear and the mode-coupled (i.e., non-linear) contributions to v_4 depends on two- and four-particle correlations. Therefore, it is instructive to investigate the model's potential to simulate the experimental measurements of two- and four-particle flow harmonics [78,79]. Figures 1 and 2 show a comparison of the centrality dependence of $v_n\{2\}$ and $v_2\{4\}$ in Au–Au collisions at 200 (a), 39 (b), 27 (c) and 19.6 (d) GeV according to the AMPT model. The AMPT calculations exhibited sensitivity to beam energy change and harmonic order n. They also indicated similar patterns to the data reported by the STAR experiment [78,79] (solid points). The data model comparisons suggest that the AMPT model contains the proper ingredient to describe the experimental data.

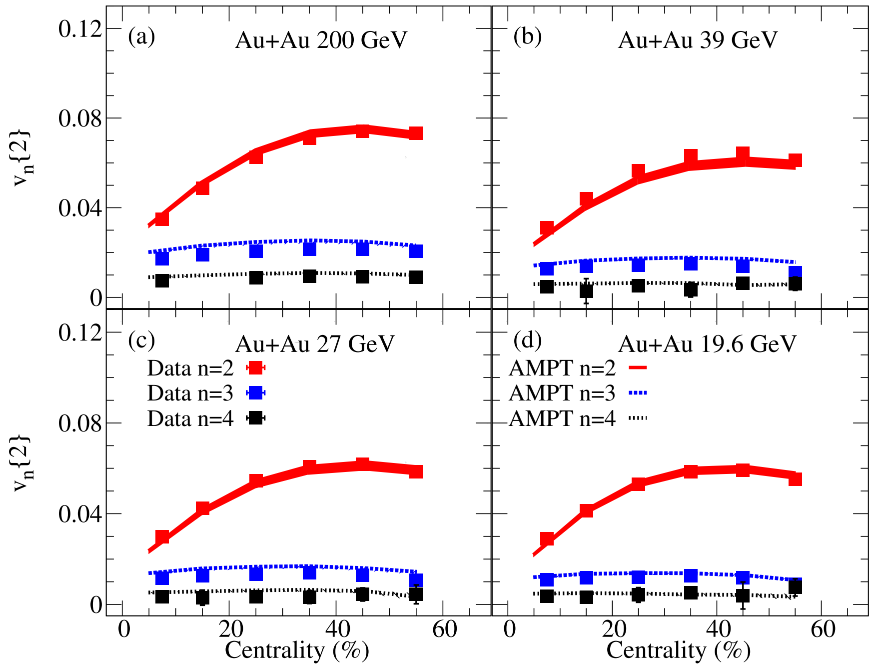

Figure 1. Comparison of the experimental and simulated centrality and beam energy dependence of $v_n\{2\}$ in Au+Au collisions at 200 GeV (panel (**a**)), 39 GeV (panel (**b**)), 27 GeV (panel (**c**)) and 19.6 GeV (panel (**d**)). The solid points represent the experimental data reported by the STAR collaboration [78,79].

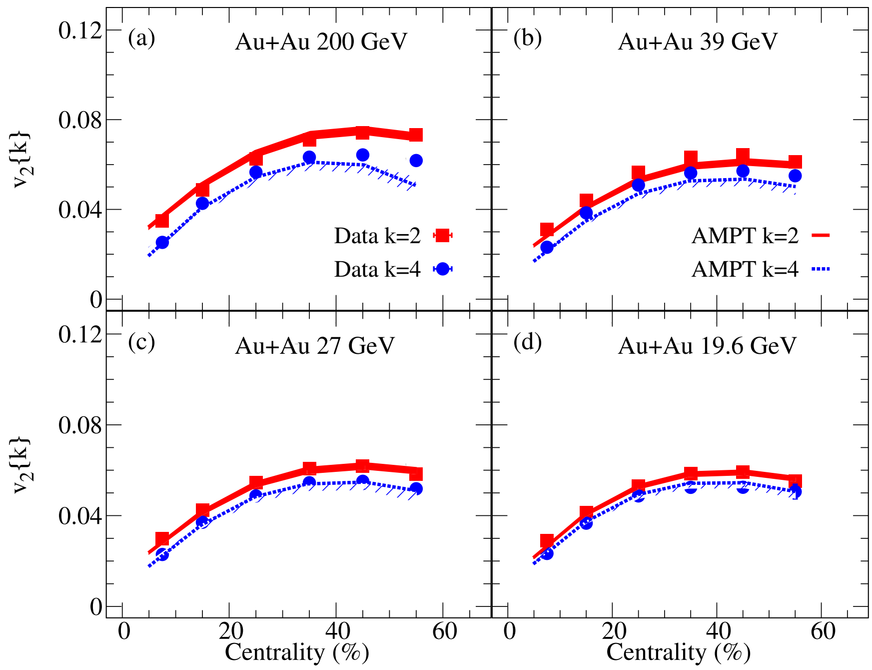

Figure 2. Centrality dependence of $v_2\{k\}$ in Au+Au collisions at 200 GeV (panel (**a**)), 39 GeV (panel (**b**)), 27 GeV (panel (**c**)) and 19.6 GeV (panel (**d**)). The solid points represent the experimental data reported by the STAR collaboration [78,79].

The centrality dependence of the three-particle correlators, $C_{4,22}$ (panel (a)) and $C_{5,23}$ (panel (b)), are shown in Figure 3 for Au+Au collisions at 200, 39, 27 and 19.6 GeV according to the AMPT model. My results demonstrate that $C_{4,22}$ and $C_{5,23}$ depend on beam energy.

These dependencies indicate that $C_{4,22}$ and $C_{5,23}$ are susceptible to the change in viscous attenuation according to the AMPT model (i.e., $\langle p_T \rangle$ and charged particle multiplicity) and initial-state eccentricity. My results reflect the capability of the three-particle correlators to constrain the interplay between the final- and initial-state effects in the AMPT model. The AMPT calculations qualitatively reproduced the trend observed in the experimental data [10]. However, the AMPT model overestimated $C_{4,22}$ for centrality larger than 30% and $C_{5,23}$ for mid-central (10–50%) region values.

Figure 4 shows the centrality and beam energy dependence of inclusive (a), mode-coupled and linear v_4 in Au+Au collisions according to the AMPT model. My results indicate that the linear contribution is the dominant contribution to inclusive v_4 in central collisions at all presented energies. In addition, v_4^{Linear} showed weak centrality dependence. In addition, the difference between linear and mode-coupled v_4 in central collisions is derived from the difference in ε_4 and ε^2, respectively. The presented results show that inclusive, linear and mode-coupled v_4 are sensitive to beam energy variation. The AMPT results are in qualitative agreement with the experimental measurements from the STAR experiment in Au+Au collisions at $\sqrt{s_N N}$ = 200 GeV [10,80].

Mode-coupling response coefficient $\chi_{4,22}$, which gives the coupling strength between lower and higher flow harmonics, is presented in Figure 5a as a function of centrality for Au+Au at 200, 39, 27 and 19.6 GeV. The $\chi_{4,22}$ calculations indicated weak centrality and beam energy dependence, which implies that (i) $\chi_{4,22}$ is dominated by initial-state eccentricity couplings and (ii) mode-coupled v_4 centrality and energy dependence arise from lower-order flow harmonics. Figure 5b illustrates the centrality and energy dependence of the correlation between flow symmetry planes, $\rho_{4,22}$, in Au+Au collisions at $\sqrt{s_{NN}}$ = 200, 39, 27 and 19.6 GeV according to the AMPT model. The AMPT calculations of $\rho_{4,22}$ indicated stronger event plane correlations in peripheral collisions at all presented energies. Nevertheless, $\rho_{4,22}$ magnitudes were shown to be independent of beam energies. Such observation implies that initial-state eccentricity direction correlations dominate the correlation between flow symmetry planes. In addition, these calculations are in agreement with the STAR experiment measurements in Au+Au collisions at $\sqrt{s_N N}$ = 200 GeV [10,80].

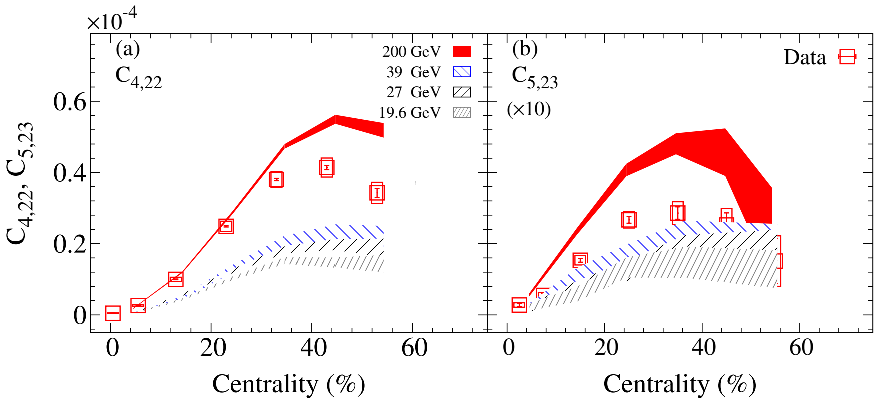

Figure 3. Centrality and beam energy dependence of three-particle correlators $C_{4,22}$ panel (**a**) and $C_{5,23}$ panel (**b**) in Au+Au collisions according to the AMPT model. The points represent the experimental measurements at 200 GeV [10].

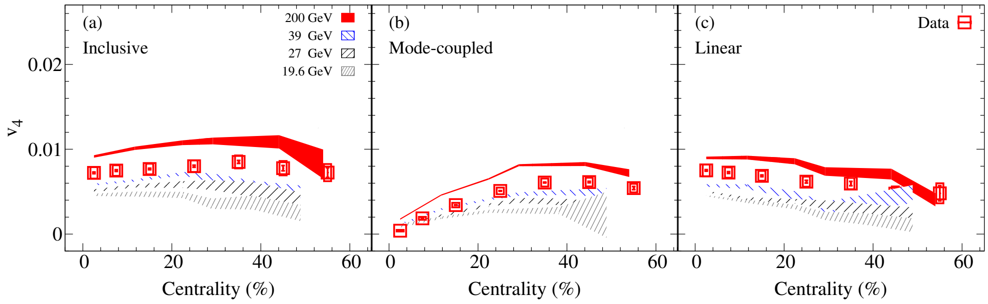

Figure 4. Centrality and beam energy dependence of inclusive, non-linear and linear v_4 panels (**a**–**c**) obtained with the two-sub-event cumulant method in Au–Au collisions at 200 GeV according to the AMPT model. The points represent the experimental measurements at 200 GeV [10].

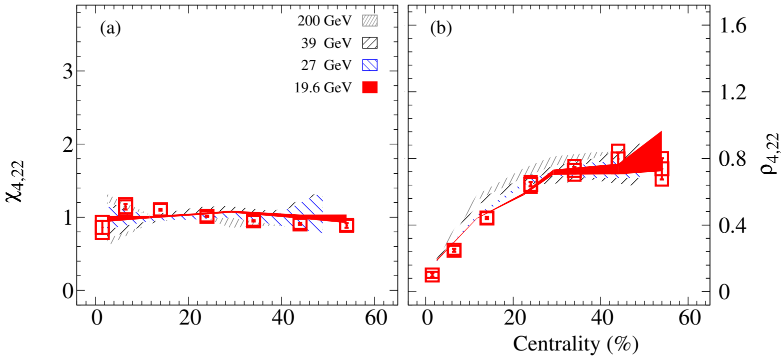

Figure 5. Comparison of $\chi_{4,22}$ panel (**a**) and $\rho_{4,22}$ panel (**b**) in Au–Au collisions at 200, 39, 27 and 19.6 GeV as functions of centrality obtained with the AMPT model. The points represent the experimental measurements at 200 GeV [10].

4. Conclusions

I have presented comprehensive AMPT model calculations to evaluate the beam energy dependence of the linear and mode-coupling contributions to v_4, $\chi_{4,22}$ and $\rho_{4,22}$. The AMPT calculations indicate similar patterns and values to the experimental measurements of $v_n\{2\}$ and $v_2\{4\}$. The AMPT calculations of mode-coupled v_4 indicate strong centrality dependence; however, they show weak centrality dependence for linear v_4. In addition, three-particle correlations and v_4 show strong beam energy dependence. In contrast, $\chi_{4,22}$ and $\rho_{4,22}$ show magnitudes and trends that are weakly dependent on beam energy. The AMPT model calculations suggest that initial-state effects might be the dominant factors behind the correlations of event plane angles and the non-linear response coefficients.

Funding: This research was supported by the US Department of Energy, Office of Nuclear Physics (DOE NP) under contract DE-FG02-87ER40331.A008.

Data Availability Statement: Not applicable.

Conflicts of Interest: The author declares no conflict of interest.

References

1. Shuryak, E.V. Quark-Gluon Plasma and Hadronic Production of Leptons, Photons and Psions. *Phys. Lett. B* **1978**, *78*, 150. [CrossRef]
2. Shuryak, E.V. Quantum Chromodynamics and the Theory of Superdense Matter. *Phys. Rep.* **1980**, *61*, 71–158. [CrossRef]
3. Muller, B.; Schukraft, J.; Wyslouch, B. First Results from Pb+Pb collisions at the LHC. *Ann. Rev. Nucl. Part. Sci.* **2012**, *62*, 361–386. [CrossRef]
4. Shuryak, E. Why does the quark gluon plasma at RHIC behave as a nearly ideal fluid? *Prog. Part. Nucl. Phys.* **2004**, *53*, 273–303. [CrossRef]

5. Romatschke, P.; Romatschke, U. Viscosity Information from Relativistic Nuclear Collisions: How Perfect is the Fluid Observed at RHIC? *Phys. Rev. Lett.* **2007**, *99*, 172301. [CrossRef] [PubMed]
6. Luzum, M.; Romatschke, P. Conformal Relativistic Viscous Hydrodynamics: Applications to RHIC results at $\sqrt{s_{NN}}$ = 200-GeV. *Phys. Rev.* **2008**, *C78*, 034915.
7. Bozek, P. Bulk and shear viscosities of matter created in relativistic heavy-ion collisions. *Phys. Rev. C* **2010**, *81*, 034909. [CrossRef]
8. Acharya, S. et al. [ALICE Collaboration] Investigations of Anisotropic Flow Using Multiparticle Azimuthal Correlations in pp, p-Pb, Xe-Xe, and Pb-Pb Collisions at the LHC. *Phys. Rev. Lett.* **2019**, *123*, 142301. [CrossRef]
9. Acharya, S. et al. [ALICE Collaboration] Higher harmonic non-linear flow modes of charged hadrons in Pb-Pb collisions at $\sqrt{s_{NN}}$ = 5.02 TeV. *JHEP* **2020**, *5*, 85. [CrossRef]
10. Adam, J. et al. [STAR Collaboration] Investigation of the linear and mode-coupled flow harmonics in Au+Au collisions at $\sqrt{s_{NN}}$ = 200 GeV. *Phys. Lett.* **2020**, *B809*, 135728. [CrossRef]
11. Heinz, U.W.; Kolb, P.F. Early thermalization at RHIC. *Nucl. Phys.* **2002**, *A702*, 269–280. [CrossRef]
12. Hirano, T.; Heinz, U.W.; Kharzeev, D.; Lacey, R.; Nara, Y. Hadronic dissipative effects on elliptic flow in ultrarelativistic heavy-ion collisions. *Phys. Lett.* **2006**, *B636*, 299–304. [CrossRef]
13. Huovinen, P.; Kolb, P.F.; Heinz, U.W.; Ruuskanen, P.V.; Voloshin, S.A. Radial and elliptic flow at RHIC: Further predictions. *Phys. Lett.* **2001**, *B503*, 58–64. [CrossRef]
14. Hirano, T.; Tsuda, K. Collective flow and two pion correlations from a relativistic hydrodynamic model with early chemical freeze out. *Phys. Rev.* **2002**, *C66*, 054905. [CrossRef]
15. Luzum, M. Flow fluctuations and long-range correlations: Elliptic flow and beyond. *J. Phys.* **2011**, *G38*, 124026. [CrossRef]
16. Song, H.; Bass, S.A.; Heinz, U.; Hirano, T.; Shen, C. 200 A GeV Au+Au collisions serve a nearly perfect quark-gluon liquid. *Phys. Rev. Lett.* **2011**, *106*, 192301. Erratum: *Phys. Rev. Lett.* **2012**, *109*, 139904. [CrossRef] [PubMed]
17. Qian, J.; Heinz, U.W.; Liu, J. Mode-coupling effects in anisotropic flow in heavy-ion collisions. *Phys. Rev.* **2016**, *C93*, 064901. [CrossRef]
18. Magdy, N. Beam energy dependence of the anisotropic flow coefficients v_n. *PoS* **2018**, *CPOD2017*, 005.
19. Magdy, N. Viscous Damping of Anisotropic Flow in 7.7 − 200 GeV Au+Au Collisions. *J. Phys. Conf. Ser.* **2017**, *779*, 012060. [CrossRef]
20. Schenke, B.; Jeon, S.; Gale, C. Anisotropic flow in $\sqrt{s} = 2.76$ TeV Pb+Pb collisions at the LHC. *Phys. Lett.* **2011**, *B702*, 59–63. [CrossRef]
21. Teaney, D.; Yan, L. Non linearities in the harmonic spectrum of heavy ion collisions with ideal and viscous hydrodynamics. *Phys. Rev.* **2012**, *C86*, 044908. [CrossRef]
22. Gardim, F.G.; Grassi, F.; Luzum, M.; Ollitrault, J.Y. Anisotropic flow in event-by-event ideal hydrodynamic simulations of $\sqrt{s_{NN}} = 200$ GeV Au+Au collisions. *Phys. Rev. Lett.* **2012**, *109*, 202302. [CrossRef] [PubMed]
23. Lacey, R.A.; Reynolds, D.; Taranenko, A.; Ajitanand, N.N.; Alexander, J.M.; Liu, F.H.; Gu, Y.; Mwai, A. Acoustic scaling of anisotropic flow in shape-engineered events: Implications for extraction of the specific shear viscosity of the quark gluon plasma. *J. Phys.* **2016**, *G43*, 10LT01. [CrossRef]
24. Alver, B.H.; Gombeaud, C.; Luzum, M.; Ollitrault, J.Y. Triangular flow in hydrodynamics and transport theory. *Phys. Rev.* **2010**, *C82*, 034913. [CrossRef]
25. Petersen, H.; Qin, G.Y.; Bass, S.A.; Muller, B. Triangular flow in event-by-event ideal hydrodynamics in Au+Au collisions at $\sqrt{s_{NN}} = 200\ A$ GeV. *Phys. Rev.* **2010**, *C82*, 041901. [CrossRef]
26. Lacey, R.A.; Wei, R.; Ajitanand, N.N.; Taranenko, A. Initial eccentricity fluctuations and their relation to higher-order flow harmonics. *Phys. Rev.* **2011**, *C83*, 044902. [CrossRef]
27. Teaney, D.; Yan, L. Triangularity and Dipole Asymmetry in Heavy Ion Collisions. *Phys. Rev.* **2011**, *C83*, 064904. [CrossRef]
28. Qiu, Z.; Heinz, U.W. Event-by-event shape and flow fluctuations of relativistic heavy-ion collision fireballs. *Phys. Rev.* **2011**, *C84*, 024911. [CrossRef]
29. Bhalerao, R.S.; Ollitrault, J.Y.; Pal, S. Characterizing flow fluctuations with moments. *Phys. Lett.* **2015**, *B742*, 94–98. [CrossRef]
30. Yan, L.; Ollitrault, J.Y. $\nu_4, \nu_5, \nu_6, \nu_7$: Nonlinear hydrodynamic response versus LHC data. *Phys. Lett.* **2015**, *B744*, 82–87. [CrossRef]
31. Poskanzer, A.M.; Voloshin, S.A. Methods for analyzing anisotropic flow in relativistic nuclear collisions. *Phys. Rev.* **1998**, *C58*, 1671–1678. [CrossRef]
32. Adam, J. et al. [STAR Collaboration] Correlation Measurements Between Flow Harmonics in Au+Au Collisions at RHIC. *Phys. Lett.* **2018**, *B783*, 459–465. [CrossRef]
33. Adam, J. et al. [ALICE collaboration] Correlated event-by-event fluctuations of flow harmonics in Pb-Pb collisions at $\sqrt{s_{_{NN}}} = 2.76$ TeV. *Phys. Rev. Lett.* **2016**, *117*, 182301. [CrossRef]
34. Adamczyk, L. et al. [STAR Collaboration] Harmonic decomposition of three-particle azimuthal correlations at energies available at the BNL Relativistic Heavy Ion Collider. *Phys. Rev.* **2018**, *C98*, 034918. [CrossRef]
35. Adare, A. et al. [PHENIX Collaboration] Measurements of Higher-Order Flow Harmonics in Au+Au Collisions at $\sqrt{s_{NN}} = 200$ GeV. *Phys. Rev. Lett.* **2011**, *107*, 252301. [CrossRef]
36. Aad, G. et al. [ATLAS Collaboration] Measurement of event-plane correlations in $\sqrt{s_{NN}} = 2.76$ TeV lead-lead collisions with the ATLAS detector. *Phys. Rev.* **2014**, *C90*, 024905. [CrossRef]

37. Aguilar-Saavedra, J.A. et al. [ATLAS Collaboration] Measurement of the correlation between flow harmonics of different order in lead-lead collisions at $\sqrt{s_{NN}}$ = 2.76 TeV with the ATLAS detector. *Phys. Rev.* **2015**, *C92*, 034903. [CrossRef]
38. Magdy, N. Collision system and beam energy dependence of anisotropic flow fluctuations. *Nucl. Phys.* **2019**, *A982*, 255–258. [CrossRef]
39. Alver, B.; Back, B.B.; Baker, M.; Ballintijn, M.; Barton, D.S.; Betts, R.R.; Bindel, R.; Busza, W.; Chetluru, V.; Garcia, E.; et al. Importance of correlations and fluctuations on the initial source eccentricity in high-energy nucleus-nucleus collisions. *Phys. Rev.* **2008**, *C77*, 014906. [CrossRef]
40. Alver, B. et al. [PHOBOS Collaboration] Non-flow correlations and elliptic flow fluctuations in gold-gold collisions at $\sqrt{s_{NN}} = 200$ GeV. *Phys. Rev.* **2010**, *C81*, 034915. [CrossRef]
41. Ollitrault, J.Y.; Poskanzer, A.M.; Voloshin, S.A. Effect of flow fluctuations and nonflow on elliptic flow methods. *Phys. Rev.* **2009**, *C80*, 014904. [CrossRef]
42. Adam, J. et al. [STAR Collaboration] Azimuthal Harmonics in Small and Large Collision Systems at RHIC Top Energies. *Phys. Rev. Lett.* **2019**, *122*, 172301. [CrossRef] [PubMed]
43. Heinz, U.; Snellings, R. Collective flow and viscosity in relativistic heavy-ion collisions. *Ann. Rev. Nucl. Part. Sci.* **2013**, *63*, 123–151. [CrossRef]
44. Magdy, N. Beam-energy dependence of the azimuthal anisotropic flow from RHIC. *arXiv* **2019**, arXiv:nucl-ex/1909.09640.
45. Adamczyk, L. et al. [STAR Collaboration] Azimuthal anisotropy in Cu+Au collisions at $\sqrt{s_{NN}}$ = 200 GeV. *Phys. Rev.* **2018**, *C98*, 014915. [CrossRef]
46. Alver, B.; Roland, G. Collision geometry fluctuations and triangular flow in heavy-ion collisions. *Phys. Rev.* **2010**, *C81*, 054905. Erratum: *Phys. Rev. C* **2010**, *82*, 039903. [CrossRef]
47. Chatrchyan, S.; Khachatryan, V.; Sirunyan, A.M.; Tumasyan, A.; Adam, W.; Bergauer, T.; Dragicevic, M.; Eroe, J.; Fabjan, C.; Friedl, M.; et al. Measurement of higher-order harmonic azimuthal anisotropy in PbPb collisions at $\sqrt{s_{NN}}$ = 2.76 TeV. *Phys. Rev.* **2014**, *C89*, 044906. [CrossRef]
48. Gardim, F.G.; Grassi, F.; Luzum, M.; Ollitrault, J.Y. Mapping the hydrodynamic response to the initial geometry in heavy-ion collisions. *Phys. Rev. C* **2012**, *85*, 024908. [CrossRef]
49. Bilandzic, A.; Christensen, C.H.; Gulbrandsen, K.; Hansen, A.; Zhou, Y. Generic framework for anisotropic flow analyses with multiparticle azimuthal correlations. *Phys. Rev.* **2014**, *C89*, 064904. [CrossRef]
50. Zhou, Y. Review of anisotropic flow correlations in ultrarelativistic heavy-ion collisions. *Adv. High Energy Phys.* **2016**, *2016*, 9365637. [CrossRef]
51. Qiu, Z.; Heinz, U. Hydrodynamic event-plane correlations in Pb+Pb collisions at $\sqrt{s} = 2.76$ ATeV. *Phys. Lett.* **2012**, *B717*, 261–265. [CrossRef]
52. Teaney, D.; Yan, L. Event-plane correlations and hydrodynamic simulations of heavy ion collisions. *Phys. Rev.* **2014**, *C90*, 024902. [CrossRef]
53. Niemi, H.; Eskola, K.J.; Paatelainen, R. Event-by-event fluctuations in a perturbative QCD + saturation + hydrodynamics model: Determining QCD matter shear viscosity in ultrarelativistic heavy-ion collisions. *Phys. Rev.* **2016**, *C93*, 024907. [CrossRef]
54. Zhou, Y.; Xiao, K.; Feng, Z.; Liu, F.; Snellings, R. Anisotropic distributions in a multiphase transport model. *Phys. Rev.* **2016**, *C93*, 034909. [CrossRef]
55. Sirunyan, A.M. et al. [CMS Collaboration] Mixed higher-order anisotropic flow and nonlinear response coefficients of charged particles in PbPb collisions at $\sqrt{s_{NN}} = 2.76$ and 5.02 TeV. *Eur. Phys. J. C* **2020**, *80*, 534. [CrossRef]
56. Lin, Z.W.; Ko, C.M.; Li, B.A.; Zhang, B.; Pal, S. A Multi-phase transport model for relativistic heavy ion collisions. *Phys. Rev.* **2005**, *C72*, 064901. [CrossRef]
57. Ma, G.L.; Lin, Z.W. Predictions for $\sqrt{s_{NN}} = 5.02$ TeV Pb+Pb Collisions from a Multi-Phase Transport Model. *Phys. Rev.* **2016**, *C93*, 054911. [CrossRef]
58. Ma, G.L. Decomposition of the jet fragmentation function in high-energy heavy-ion collisions. *Phys. Rev.* **2013**, *C88*, 021902. [CrossRef]
59. Ma, G.L. Medium modifications of jet shapes in Pb+Pb collisions at $\sqrt{s_{NN}}$ = 2.76 TeV within a multiphase transport model. *Phys. Rev.* **2014**, *C89*, 024902. [CrossRef]
60. Bzdak, A.; Ma, G.L. Elliptic and triangular flow in p+Pb and peripheral Pb+Pb collisions from parton scatterings. *Phys. Rev. Lett.* **2014**, *113*, 252301. [CrossRef]
61. Nie, M.W.; Huo, P.; Jia, J.; Ma, G.L. Multiparticle azimuthal cumulants in p+Pb collisions from a multiphase transport model. *Phys. Rev.* **2018**, *C98*, 034903. [CrossRef]
62. Magdy, N.; Nie, M.W.; Huang, L.; Ma, G.L.; Lacey, R.A. An extended $R^{(2)}_{\Psi_m}(\Delta S_2)$ correlator for detecting and characterizing the Chiral Magnetic Wave. *Phys. Lett. B* **2020**, *811*, 135986. . [CrossRef]
63. Magdy, N. Characterizing the initial and final state effects of relativistic nuclear collisions. *Phys. Rev. C* **2022**, *107*, 024905. [CrossRef]
64. Magdy, N. Measuring differential flow angle fluctuations in relativistic nuclear collisions. *Phys. Rev. C* **2022**, *106*, 044911. [CrossRef]
65. Magdy, N. Impact of nuclear deformation on collective flow observables in relativistic U+U collisions. *arXiv* **2022**, arXiv:2206.05332.

66. Zhang, B. ZPC 1.0.1: A Parton cascade for ultrarelativistic heavy ion collisions. *Comput. Phys. Commun.* **1998**, *109*, 193–206. [CrossRef]
67. Wang, X.N.; Gyulassy, M. HIJING: A Monte Carlo model for multiple jet production in p p, p A and A A collisions. *Phys. Rev.* **1991**, *D44*, 3501–3516. [CrossRef]
68. Gyulassy, M.; Wang, X.N. HIJING 1.0: A Monte Carlo program for parton and particle production in high-energy hadronic and nuclear collisions. *Comput. Phys. Commun.* **1994**, *83*, 307. [CrossRef]
69. Li, B.A.; Ko, C.M. Formation of superdense hadronic matter in high-energy heavy ion collisions. *Phys. Rev.* **1995**, *C52*, 2037–2063. [CrossRef]
70. Xu, J.; Ko, C.M. Pb-Pb collisions at $\sqrt{s_{NN}} = 2.76$ TeV in a multiphase transport model. *Phys. Rev. C* **2011**, *83*, 034904. [CrossRef]
71. Nasim, M. Systematic study of symmetric cumulants at $\sqrt{s_{NN}}$ = 200 GeV in Au+Au collision using transport approach. *Phys. Rev. C* **2017**, *95*, 034905. . [CrossRef]
72. Solanki, D.; Sorensen, P.; Basu, S.; Raniwala, R.; Nayak, T.K. Beam energy dependence of Elliptic and Triangular flow with the AMPT model. *Phys. Lett. B* **2013**, *720*, 352–357. [CrossRef]
73. Bilandzic, A.; Snellings, R.; Voloshin, S. Flow analysis with cumulants: Direct calculations. *Phys. Rev.* **2011**, *C83*, 044913. [CrossRef]
74. Jia, J.; Zhou, M.; Trzupek, A. Revealing long-range multiparticle collectivity in small collision systems via subevent cumulants. *Phys. Rev.* **2017**, *C96*, 034906. [CrossRef]
75. Gajdošová, K. Investigations of anisotropic collectivity using multi-particle correlations in pp, p–Pb and Pb–Pb collisions. *Nucl. Phys.* **2017**, *A967*, 437–440. [CrossRef]
76. Magdy, N.; Evdokimov, O.; Lacey, R.A. A method to test the coupling strength of the linear and nonlinear contributions to higher-order flow harmonics via Event Shape Engineering. *J. Phys. G* **2020**, *48*, 025101. [CrossRef]
77. Bhalerao, R.S.; Ollitrault, J.Y.; Pal, S. Event-plane correlators. *Phys. Rev.* **2013**, *C88*, 024909. [CrossRef]
78. Adams, J. et al. [STAR Collaboration] Azimuthal anisotropy in Au+Au collisions at $\sqrt{s_{NN}}$ = 200-GeV. *Phys. Rev. C* **2005**, *72*, 014904. [CrossRef]
79. Adamczyk, L. et al. [STAR Collaboration] Beam Energy Dependence of the Third Harmonic of Azimuthal Correlations in Au+Au Collisions at RHIC. *Phys. Rev. Lett.* **2016**, *116*, 112302. [CrossRef]
80. Aboona, B.E. et al. [STAR Collaboration] Beam energy dependence of the linear and mode-coupled flow harmonics in Au+Au collisions. *Phys. Lett. B* **2023**, *137755*, 0370–2693. [CrossRef]